

©The Royal Society of Chemistry 2015

Electronic Supplementary Information (ESI) for Soft Matter: *Anomalous energy cascades in dense granular materials yielding under simple shear deformations*

Kuniyasu Saitoh* and Hideyuki Mizuno†

December 18, 2015

Abstract

In this Electronic Supplementary Information (ESI), we provide the supplementary information about the manuscript. In Sec. 1, we summarize the rheology of dense granular materials and explain a continuum theory proposed by Savage [1]. In Sec. 2, we derive a theoretical expression of the spectrum of non-affine velocities. In Sec. 3, we clarify the difference between usual energy cascade and the cascade of kinetic energy observed in dense granular flows. In Sec. 4, we show some supplementary data of molecular dynamics (MD) simulations.

1 Dense granular rheology

In this section, we briefly introduce the rheology of granular materials and continuum descriptions of dense granular flows. Especially, we focus on a continuum theory proposed by Savage [1], where usual hydrodynamic equations (Secs. 1.1 and 1.2) with a constitutive model characteristic of dense granular flows (Sec. 1.3) are explained in detail. We discuss different models of pair correlation function at contact (Sec. 1.4), which is an ingredient of the constitutive model, and validate the hydrodynamic equations by MD simulations (Secs. 1.5-1.7).

The rheology of granular materials is strongly affected by the volume fraction (or area fraction in two dimensions) of granular particles, ϕ_0 [2–8]. If the fraction is sufficiently small, the system behaves like a gas, where *kinetic theory* succeeds in describing the flow behavior [9–17]. However, if the fraction exceeds a critical value, *contact forces* between granular particles also contribute to the flow properties [1, 18]. Figure 1 displays a sketch of *flow curves* of granular materials, i.e. the shear stress, σ , plotted against the shear rate, $\dot{\gamma}$: Below the critical density, $\phi_0 < \phi_c$ (the dotted line in Fig.

1), the Bagnold scaling predicted by kinetic theory, $\sigma \sim \dot{\gamma}^2$, well describes the flow behavior. In such an *unjammed state*, the shear stress goes to zero in a quasi-static limit, $\dot{\gamma} \rightarrow 0$, where *glassy dynamics* of granular particles have been extensively investigated [19–26]. On the other hand, it remains finite above the critical density, $\phi_0 > \phi_c$ (the solid line in Fig. 1), so that the system exhibits the *yield stress*, where many constitutive models for such a *yielding* (or *jammed*) state have been proposed, e.g. the μ - I rheology [27–33], non-local models for slow flows [34–36], and order-parameter descriptions for fluid-solid coexistent flows [37–45]. Note that the shear stress of jammed granular materials is *rate-independent* in a quasi-static regime, $\dot{\gamma} \ll 1$, i.e. the so-called *critical-state* in soil mechanics [46], while the rate-dependent kinetic contribution to the shear stress becomes important in a rapid-flow regime (Fig. 1). In addition, the discontinuous shear thickening, i.e. a jump from unjammed state to yielding state, is also possible for frictional granular materials [47–51].

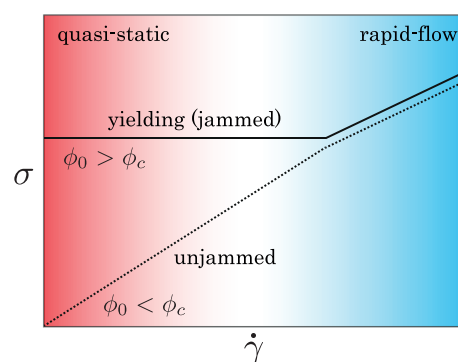


Figure 1: (Color online) A sketch of flow curves of granular materials (in a double logarithmic scale): In unjammed state, $\phi_0 < \phi_c$ (the dotted line), the Bagnold scaling, $\sigma \sim \dot{\gamma}^2$, well describes the flow behavior, while the system exhibits finite yield stress in yielding (or jammed) state, $\phi_0 > \phi_c$ (the solid line). In quasi-static regime, $\dot{\gamma} \ll 1$, the shear stress of jammed granular materials is *rate-independent* (the solid line), while the rate-dependent kinetic contribution to the shear stress becomes important in rapid-flow regime.

*Faculty of Engineering Technology, MESA+, University of Twente, Drienerlolaan 5, 7522 NB, Enschede, The Netherlands. E-mail: k.saitoh@utwente.nl

†Institut für Materialphysik im Weltraum, Deutsches Zentrum für Luft- und Raumfahrt (DLR), 51170 Köln, Germany. E-mail: Hideyuki.Mizuno@dlr.de

1.1 Savage's continuum theory

To describe the complicated rheology of dense granular materials, we adopt a continuum theory proposed by Savage [1]. In his original paper, Ref. [1], he considered granular flows in two-dimension, where the density of granular particles is high and the shear rate applied to the system is very small so that the basic assumption of kinetic theory (i.e. binary collisions and the molecular chaos) is violated. To provide constitutive relations for such dense granular flows, he adopted the *associated flow rule*: The *plastic potential* is assumed to be equal to the *yield function* in the mean-stress and stress-difference plane. In soil mechanics, it is known that the associated flow rule is quite useful if the principal axes of stress and strain (rate) coincide. Adopting the von Mises type yield criterion (i.e. the yield function is given by a circle) and differentiating the plastic potential, he derived hydrodynamic equations for compressive and frictional granular materials. In his theory, transport coefficients are formulated such that they are consistent with the kinetic theory of two-dimensional granular gases [11].

The hydrodynamic equations derived by Savage include the continuity equation, equation of momentum conservation, and equation of granular temperature as

$$\frac{D\rho}{D\tilde{t}} = -\rho\tilde{\nabla}_i\tilde{u}_i, \quad (1)$$

$$\rho\frac{D\tilde{u}_i}{D\tilde{t}} = \tilde{\nabla}_j\tilde{\sigma}_{ij}, \quad (2)$$

$$n\frac{DT}{D\tilde{t}} = \tilde{\sigma}_{ij}\tilde{\nabla}_i\tilde{u}_j - \tilde{\nabla}_i\tilde{q}_i - \tilde{\chi}, \quad (3)$$

respectively. Here, hydrodynamic fields are introduced as the mass density, $\rho = mn$, velocity field, \tilde{u}_i , and granular temperature, T , where m , n , and i ($= \tilde{x}, \tilde{y}$) represent the particle mass, number density, and each coordinate, respectively. On the right-hand-sides, the Einstein convention is used for the subscripts, i and j ($= \tilde{x}, \tilde{y}$). On the left-hand-sides, the material derivative is defined as $D/D\tilde{t} \equiv \partial/\partial\tilde{t} + \tilde{u}_i\tilde{\nabla}_i$ with the time derivative, $\partial/\partial\tilde{t}$, and gradient, $\tilde{\nabla}_i$. Constitutive relations for the stress tensor, $\tilde{\sigma}_{ij}$, and heat flux, \tilde{q}_i , are given by the usual forms,

$$\tilde{\sigma}_{ij} = \tilde{\eta}(\tilde{\nabla}_i\tilde{u}_j + \tilde{\nabla}_j\tilde{u}_i) + \delta_{ij}(\tilde{\xi} - \tilde{\eta})\tilde{\nabla}_l\tilde{u}_l - \delta_{ij}\tilde{p}, \quad (4)$$

$$\tilde{q}_i = -\tilde{\kappa}\tilde{\nabla}_i T, \quad (5)$$

respectively ($l = \tilde{x}, \tilde{y}$), where the pressure, shear viscosity, bulk viscosity, and thermal conductivity are introduced as \tilde{p} , $\tilde{\eta}$, $\tilde{\xi}$, and $\tilde{\kappa}$, respectively. Note that the last term on the right-hand-side of Eq. (3), i.e. $\tilde{\chi} \equiv nT\tilde{\zeta}$, represents the *energy dissipation* in the bulk due to inelastic interactions between granular particles, where $\tilde{\zeta}$ is defined as a dissipation rate.

1.2 Nondimensionalization

We introduce scaling units of mass, length, and time as the particle mass, m , mean diameter, d_m , and *microscopic time scale*, $t_m \equiv \eta_n/k_n$, respectively, where k_n and η_n are respectively the normal spring constant and viscosity coefficient for

the model of granular particles in MD simulations. For example, the shear rate, $\dot{\gamma}$, is nondimensionalized as $s \equiv \dot{\gamma}t_m$. Then, we nondimensionalize the stress tensor, pressure, and heat flux as $\sigma_{ij} \equiv (\nu/\varepsilon)\tilde{\sigma}_{ij}$, $p \equiv (\nu/\varepsilon)\tilde{p}$, and $q_i \equiv (d_m t_m/\varepsilon)\tilde{q}_i$, respectively, where $\nu \equiv d_m^2$ and $\varepsilon \equiv m(d_m/t_m)^2$ are the particle area and an energy unit, respectively. The transport coefficients and dissipation rate are also nondimensionalized as $\eta \equiv (t_m/m)\tilde{\eta}$, $\xi \equiv (t_m/m)\tilde{\xi}$, $\kappa \equiv t_m\tilde{\kappa}$, and $\zeta \equiv t_m\tilde{\zeta}$, respectively. Therefore, introducing a dimensionless time derivative, $\partial/\partial t \equiv t_m\partial/\partial\tilde{t}$, dimensionless coordinates, $x \equiv \tilde{x}/d_m$ and $y \equiv \tilde{y}/d_m$, and dimensionless gradient, $\nabla_i \equiv d_m\tilde{\nabla}_i$, we nondimensionalize the hydrodynamic equations (1)-(3) as

$$\frac{D\phi}{Dt} = -\phi\nabla_i u_i, \quad (6)$$

$$\phi\frac{Du_i}{Dt} = \nabla_j\sigma_{ij}, \quad (7)$$

$$\phi\frac{D\theta}{Dt} = \sigma_{ij}\nabla_i u_j - \nabla_i q_i - \chi, \quad (8)$$

respectively, where we have introduced the dimensionless material derivative, $D/Dt \equiv \partial/\partial t + u_i\nabla_i$, and dimensionless energy dissipation, $\chi \equiv \phi\theta\zeta$. Here, the hydrodynamic fields are nondimensionalized as the area fraction, $\phi \equiv \nu n$, dimensionless velocity field, $u_i \equiv (t_m/d_m)\tilde{u}_i$, and dimensionless granular temperature, $\theta \equiv T/\varepsilon$, respectively.

1.3 Constitutive models

To close the (dimensionless) hydrodynamic equations, we need to determine functional forms of pressure, transport coefficients, and energy dissipation by *constitutive models*.

Constitutive models for granular gases are well established by kinetic theory of inelastic particles [9–17], where the number density is assumed to be small (or the particle stiffness is sufficiently high) so that the duration of contact between granular particles can be neglected. In this case, the (dimensionless) pressure is determined by the kinetic contribution,

$$p_{\text{kin}} = [1 + (1 + e)G(\phi)]\phi\theta, \quad (9)$$

where e is the normal restitution coefficient of granular particles and the pair correlation function, $G(\phi)$, is given in later (Sec. 1.4). Similarly, the (dimensionless) bulk viscosity, shear viscosity, thermal conductivity, and energy dissipation are given by

$$\xi_{\text{kin}} = a_\xi G(\phi)\phi\theta^{1/2}, \quad (10)$$

$$\eta_{\text{kin}} = [a_\eta G(\phi) + b_\eta G(\phi)^{-1} + c_\eta]\phi\theta^{1/2}, \quad (11)$$

$$\kappa_{\text{kin}} = [a_\kappa G(\phi) + b_\kappa G(\phi)^{-1} + c_\kappa]\phi\theta^{1/2}, \quad (12)$$

$$\chi_{\text{kin}} = a_\chi G(\phi)\phi\theta^{3/2}, \quad (13)$$

respectively, with the constants listed in Table 1 [11].

In dense granular flows, however, the duration of contact cannot be neglected such that contact forces between granular particles also contribute to the stress. To include such contact contributions to the hydrodynamic equations, we adopt a

$$\begin{aligned}
a_\xi &= \frac{4(1+e)}{\pi^{3/2}} \\
a_\eta &= \frac{1+e}{\pi^{1/2}} \left[\frac{(1+e)(3e-1)}{4(7-3e)} + \frac{2}{\pi} \right] \\
b_\eta &= \frac{\pi^{1/2}(7-3e)}{(1+e)(3e+1)} \\
c_\eta &= \frac{2\pi^{1/2}(7-3e)}{(1+e)(3e+1)} \\
a_\kappa &= \frac{1+e}{\pi^{1/2}} \left[\frac{9(1+e)^2(2e-1)}{4(19-15e)} + \frac{4}{\pi} \right] \\
b_\kappa &= \frac{16}{\pi^{1/2}(1+e)(19-15e)} \\
c_\kappa &= \frac{6(2e^2+e+1)}{\pi^{1/2}(19-15e)} \\
a_\chi &= \frac{16}{\pi^{3/2}}(1-e^2)
\end{aligned}$$

Table 1: Constants for the kinetic contributions to the transport coefficients and energy dissipation, Eqs. (10)-(13).

constitutive model proposed by Savage [1]. In this model, the pressure includes the contact contribution as

$$p = p_{\text{kin}} + p_{\text{con}}, \quad (14)$$

where the contact part is defined as

$$p_{\text{con}} = a_0 \log \left(\frac{\phi_\infty - \phi_c}{\phi_\infty - \phi} \right). \quad (15)$$

The contact part is zero if the area fraction corresponds to the critical value, i.e. $\phi = \phi_c$, while it diverges if the area fraction approaches the maximum, i.e. $\phi \rightarrow \phi_\infty$. Therefore, it should be noted that the model can be used in the range between $\phi_c < \phi < \phi_\infty$. In Eq. (15), a_0 represents a reference value of pressure which we use as a fitting parameter (see Sec. 1.6).

In Savage's model, the transport coefficients and dissipation rate are also modified to include both kinetic and contact contributions: The bulk viscosity, shear viscosity, thermal conductivity, and energy dissipation are given by

$$\xi = \frac{p}{f_\xi(\phi)\theta^{1/2}}, \quad (16)$$

$$\eta = \frac{p}{f_\eta(\phi)\theta^{1/2}}, \quad (17)$$

$$\kappa = \frac{p}{f_\kappa(\phi)\theta^{1/2}}, \quad (18)$$

$$\chi = \frac{p\theta^{1/2}}{f_\chi(\phi)}, \quad (19)$$

respectively, where all the quantities have kinetic and contact parts through the complete form of pressure, $p = p_{\text{kin}} + p_{\text{con}}$. In Eqs. (16)-(19), dimensionless functions are introduced as

$$f_\xi(\phi) = \frac{1 + (1+e)G(\phi)}{a_\xi G(\phi)}, \quad (20)$$

$$f_\eta(\phi) = \frac{1 + (1+e)G(\phi)}{a_\eta G(\phi) + b_\eta G(\phi)^{-1} + c_\eta}, \quad (21)$$

$$f_\kappa(\phi) = \frac{1 + (1+e)G(\phi)}{a_\kappa G(\phi) + b_\kappa G(\phi)^{-1} + c_\kappa}, \quad (22)$$

$$f_\chi(\phi) = \frac{1 + (1+e)G(\phi)}{a_\chi G(\phi)}, \quad (23)$$

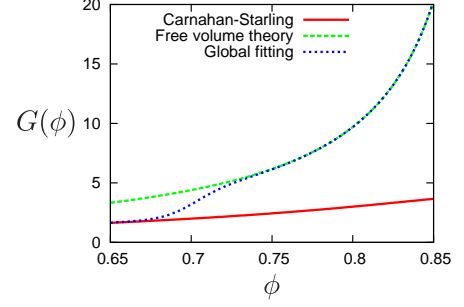


Figure 2: (Color online) Three different models of pair correlation function at contact, $G(\phi)$, where the red solid, green broken, and blue dotted lines represent the Carnahan-Starling model, $G_{\text{CS}}(\phi)$, free volume theory, $G_{\text{FV}}(\phi)$, and global fitting, $G_{\text{GF}}(\phi)$, i.e. Eqs. (24)-(26), respectively, as listed in the legend.

such that Eqs. (16)-(19) converge to the kinetic parts, Eqs. (10)-(13), respectively (e.g. $\xi \rightarrow \xi_{\text{kin}}$), in the limit of zero contact pressure, $p_{\text{con}} \rightarrow 0$ (or the onset of *unjammed*, $\phi \rightarrow \phi_c$).

1.4 Pair correlation functions

In Savage's theory, there are several choices of the *pair correlation function at contact*, $G(\phi)$, which is an ingredient of the dimensionless functions, Eq. (20)-(23). Here, we examine three different models of pair correlation function at contact, i.e. the *Carnahan-Starling model*, *free volume theory*, and *global fitting*, defined as

$$G_{\text{CS}}(\phi) = \frac{\phi(16-7\phi)}{16(1-\phi)^2}, \quad (24)$$

$$G_{\text{FV}}(\phi) = \left[(1+e) \left(\sqrt{\phi_\infty/\phi} - 1 \right) \right]^{-1}, \quad (25)$$

$$G_{\text{GF}}(\phi) = G_{\text{CS}}(\phi) + \frac{G_{\text{FV}}(\phi) - G_{\text{CS}}(\phi)}{1 + \exp[-(\phi - \phi_f)/m_f]}, \quad (26)$$

respectively [42]. It is known that the Carnahan-Starling model, $G_{\text{CS}}(\phi)$, underestimates the pair correlations in dense systems, while the free volume theory, $G_{\text{FV}}(\phi)$, overestimates them in dilute systems. Thus, the global fitting, $G_{\text{GF}}(\phi)$, proposed by Luding [52], smoothly connects the Carnahan-Starling model in low density to the free volume theory in high density, where the fitting parameters, $\phi_f = 0.7$ and $m_f = 10^{-2}$, are conventionally used [52].

Figure 2 displays the three different models of pair correlation function at contact, i.e. $G_{\text{CS}}(\phi)$, $G_{\text{FV}}(\phi)$, and $G_{\text{GF}}(\phi)$, where the normal restitution coefficient of granular particles, $e = 0.7$, and maximum area fraction, $\phi_\infty = 0.9$, are used in the free volume theory, Eq. (25). The constitutive model of pressure, Eqs. (14) and (15), can be used in the range between $\phi_c < \phi < \phi_\infty$, where a large difference between the Carnahan-Starling model and free volume theory exists (Fig. 2) and only the global fitting can describe the transition from one to another (around the transition density, $\phi = \phi_f$). Therefore, we

employ the global fitting as the model of pair correlation function at contact, i.e. $G(\phi) = G_{\text{GF}}(\phi)$, in the manuscript. In Sec. 2.3, we examine the dependence of our theoretical expression for the spectrum on the model of pair correlation function at contact.

1.5 Homogeneous solution

The dimensionless hydrodynamic equations (6)-(8) have a homogeneous solution,

$$(\phi, u_x, u_y, \theta) = (\phi_0, sy, 0, \theta_0), \quad (27)$$

where ϕ_0 is a constant (or the mean area fraction) and $s = \dot{\gamma}t_m$ is the scaled shear rate. The homogeneous granular temperature (or the mean granular temperature), θ_0 , is determined by substituting Eq. (27) to the equation of granular temperature, Eq. (8), which leads to the balance between external *supply of energy* (by simple shear deformations) and *energy dissipation* (due to inelastic interactions) as $s^2\eta = \chi$. From Eqs. (17) and (19), the mean granular temperature is found to be $\theta_0 = s^2 f_\chi(\phi_0)/f_\eta(\phi_0)$.

If we neglect small fluctuations of the hydrodynamic fields around the homogeneous solution, Eq. (27), the mean shear stress is given by $\sigma = s\eta = sp/f_\eta(\phi_0)\theta_0^{1/2}$. Therefore, the mean shear stress is divided into the kinetic and contact parts as $\sigma = \sigma_{\text{kin}} + \sigma_{\text{con}}$ because of the pressure, $p = p_{\text{kin}} + p_{\text{con}}$, where the contact part of mean shear stress is given by

$$\sigma_{\text{con}} = \frac{a_0}{\sqrt{f_\eta(\phi_0)f_\chi(\phi_0)}} \log\left(\frac{\phi_\infty - \phi_c}{\phi_\infty - \phi_0}\right). \quad (28)$$

Note that the contact parts of pressure and mean shear stress, Eqs. (15) and (28), are independent of the shear rate, i.e. they are *rate-independent*.

1.6 Input parameters

Before we validate the hydrodynamic equations (6)-(8) by MD simulations, we summarize input parameters for MD simulations, the models of pair correlation function at contact (Sec. 1.4), and the constitutive model (Sec. 1.3), where the parameter values used in the manuscript are listed in Table 2.

The dense granular rheology is governed by the two *control parameters*, i.e. the mean area fraction, ϕ_0 , and scaled shear rate, $\dot{\gamma}t_m$, which we use in both MD simulations and the theoretical analysis in Sec. 2. In our MD simulations, we have introduced the two *material constants*, i.e. the normal restitution coefficient, e , and microscopic friction coefficient, μ_m , where we fix them to $e = 0.7$ and $\mu_m = 0.5$ in the following analysis and confirm that our results are insensitive to the microscopic friction coefficient in the range between $0.1 \leq \mu_m \leq 0.5$ (see Sec. 4.2). Note that the tangential restitution coefficient, e_t , can be introduced as well, though we did not change its value in our MD simulations. The flow behavior of dense granular materials drastically change around the *critical area fraction*, ϕ_c , from unjammed states ($\phi_0 < \phi_c$) to yielding states ($\phi_0 > \phi_c$). From our results of MD simulations, the critical

e	μ_m	ϕ_c	ϕ_∞	ϕ_f	m_f	a_0/k_n
0.7	0.5	0.8	0.9	0.7	10^{-2}	3.25×10^{-2}

Table 2: Parameters for MD simulations, the models of pair correlation function at contact, and the constitutive model used in the manuscript, where $e, \mu_m, \phi_c, \phi_\infty, \phi_f, m_f$, and a_0 are the normal restitution coefficient, microscopic friction coefficient, critical area fraction, maximum area fraction, transition density, fitting parameter for $G_{\text{GF}}(\phi)$, and reference value of contact pressure, respectively.

area fraction can be estimated as, $\phi_c \simeq 0.8$, where the steady state stress suddenly increases around $\phi_0 = \phi_c$ (see Sec. 1.7).

In the models of pair correlation function at contact (Sec. 1.4), we have three *free parameters*, i.e. the maximum area fraction, ϕ_∞ , for the free volume theory, Eq. (25), and two free parameters, ϕ_f and m_f , for the global fitting, Eq. (26). From the previous studies of pair correlation function [42, 52], we conventionally use $\phi_\infty = 0.9$, $\phi_f = 0.7$, and $m_f = 10^{-2}$.

In the constitutive model of dense granular materials (Sec. 1.3), we have a *fitting parameter*, i.e. the reference value of contact pressure, a_0 , which we will determine from the fitting for the numerical results of steady state stress (see Sec. 1.7).

1.7 Macroscopic flow properties

To validate Savage's theory, we compare theoretical predictions of dense granular rheology with results of MD simulations. The hydrodynamic equations (6)-(8) can be applied to jammed granular materials ($\phi > \phi_c$) either in a quasi-static regime, where the shear rate is very small and the stress becomes *rate-independent* (the yielding state in Fig. 1), or in a rapid-flow, where the shear rate is quite high and the rate-dependent kinetic contribution to the stress becomes important. Because the shear rate used in our MD simulations is very small, we examine the rate-independent contact contribution to the stress, i.e. p_{con} and σ_{con} , where the theoretical predictions are given by Eqs. (15) and (28), respectively¹.

First, we examine the dependence of pressure and shear stress on the mean area fraction, ϕ_0 . In our MD simulations, the contact contributions to the pressure and shear stress are calculated as $p_{\text{con}}^{\text{MD}} = (\sigma_{xx} + \sigma_{yy})/2$ and $\sigma_{\text{con}}^{\text{MD}} = (\sigma_{xy} + \sigma_{yx})/2$, respectively, where the macroscopic stress tensor, $\sigma_{\alpha\beta}$ ($\alpha, \beta = x, y$), is defined as

$$\sigma_{\alpha\beta} = \frac{1}{L^2} \sum_{i < j} r_{\alpha,ij} f_{\beta,ij} \quad (29)$$

with the system area, L^2 . In Eq. (29), $\mathbf{f}_{ij} = (f_{x,ij}, f_{y,ij})$ is the *contact force* between the particles, i and j , and $\mathbf{r}_{ij} = (r_{x,ij}, r_{y,ij})$ is the relative position defined as $\mathbf{r}_{ij} \equiv \mathbf{r}_i - \mathbf{r}_j$ with the particles' positions, \mathbf{r}_i and \mathbf{r}_j . Figure 3 displays the

¹We confirmed that the kinetic contribution to the stress is $p_{\text{kin}} \simeq 3.75 \times 10^{-4}$ and $\sigma_{\text{kin}} \simeq 3.75 \times 10^{-5}$ at most in our MD simulation with the largest shear rate, $\dot{\gamma}t_m = 2.5 \times 10^{-3}$.

contact parts of (a) pressure and (b) shear stress in steady states, where the theoretical predictions (the broken lines) well describe the results of MD simulations (the open circles) if we choose the reference value in Eqs. (15) and (28) as $a_0 = 3.25 \times 10^{-2} k_n$ (we give the dimension of the spring constant, k_n , to the stress, p_{con} and σ_{con} , and reference value, a_0). In this figure, both the pressure and shear stress discontinuously increase from unjammed states, $\phi_0 < \phi_c$, to yielding states, $\phi_0 > \phi_c$, where the critical area fraction is estimated as $\phi_c \simeq 0.8$ (the vertical dotted lines in the insets).

Next, we discuss the dependence of pressure and shear stress on the scaled shear rate, $\dot{\gamma}t_m$. Figure 4 shows the contact parts of (a) pressure and (b) shear stress in steady states. In this figure, the results of MD simulations (the open circles) are almost *rate-independent* if the shear rate is small enough, $\dot{\gamma}t_m < 10^{-4}$, as the system is in a quasi-static regime, where the agreement with the continuum theory (the broken lines) is fairly well if we use the same value of a_0 with that in Fig. 3.

Therefore, the continuum theory proposed by Savage [1] well describes macroscopic flow properties of jammed granular materials ($\phi_0 > \phi_c$) in a quasi-static regime ($\dot{\gamma}t_m \ll 1$), where a good agreement with the results of MD simulations and theoretical predictions is established if the reference value in Eqs. (15) and (28) is given by

$$a_0 = 3.25 \times 10^{-2} k_n. \quad (30)$$

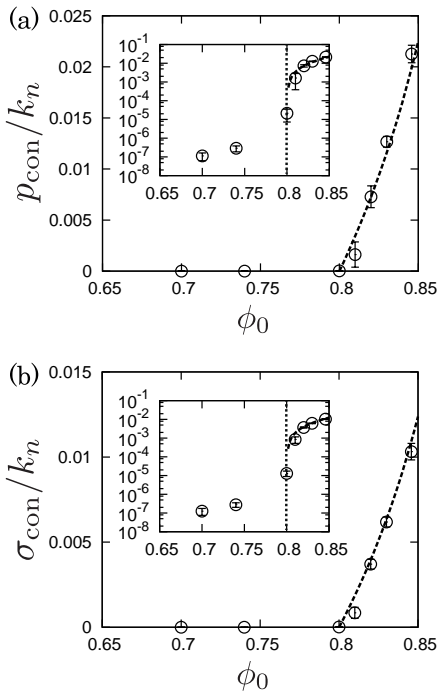


Figure 3: The dependence of contact parts of (a) pressure, p_{con} , and (b) shear stress, σ_{con} , on the mean area fraction, ϕ_0 . The open circles are the results of MD simulations, where the scaled shear rate is fixed to $\dot{\gamma}t_m = 2.5 \times 10^{-5}$. The broken lines represent the theoretical predictions, Eqs. (15) and (28), where we used the parameter values listed in Table 2.

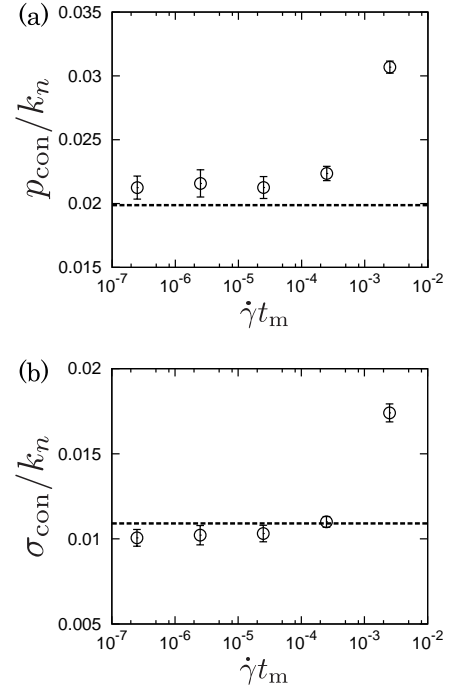


Figure 4: The dependence of contact parts of (a) pressure, p_{con} , and (b) shear stress, σ_{con} , on the scaled shear rate, $\dot{\gamma}t_m$. The open circles are the results of MD simulations, where the mean area fraction is fixed to $\phi_0 = 0.84$. The broken lines represent the theoretical predictions, Eqs. (15) and (28), where we used the parameter values listed in Table 2.

2 A theoretical expression of the spectrum of non-affine velocities

In this section, we derive a theoretical expression of the spectrum of non-affine velocities from hydrodynamic equations of dense granular materials. Because the spectrum, $E(k)$, is given by the Fourier transform of non-affine velocity field, $\delta\mathbf{u}$, our derivation includes the following procedures: (i) Assuming that $|\delta\mathbf{u}|$ is small, we linearize the hydrodynamic equations (6)-(8) around the mean velocity field. (ii) We transform the linearized hydrodynamic equations (or *linearized hydrodynamics*) into the Fourier space. (iii) To determine the Fourier component of $\delta\mathbf{u}$, we solve the linearized hydrodynamics by *perturbation theory*. (iv) We use the scaled shear rate, $\dot{\gamma}t_m$, as an expansion parameter, ϵ , for the perturbative calculations. (v) We scale the energy dissipation and wave number as $\chi \sim \epsilon^2$ and $k \sim \epsilon$, respectively. (vi) Then, the Fourier component of $\delta\mathbf{u}$, i.e. *hydrodynamic mode* of non-affine velocity field, is determined up to the first order of ϵ . Therefore, we finally obtain a theoretical expression of the spectrum, $E(k)$, which is expanded into the power series of $\epsilon = \dot{\gamma}t_m$ and is truncated at the second order of ϵ , i.e. $O(\epsilon^2)$.

In Sec. 2.1, we linearize the hydrodynamic equations by the procedures (i) and (ii). In Sec. 2.2, we solve the linearized hydrodynamics by the procedures (iii)-(vi). In Sec. 2.3, we discuss the dependence of our theoretical expression of $E(k)$

on the mean area fraction, ϕ_0 , the models of pair correlation function, $G(\phi)$, and free parameters, a_0 , ϕ_c , and ϕ_∞ .

2.1 Linearized hydrodynamics

The dimensionless hydrodynamic equations (6)-(8) have the homogeneous solution, Eq. (27), i.e. $\phi(\mathbf{r}, t) = \phi_0$, $\theta(\mathbf{r}, t) = \theta_0$, and $\mathbf{u}(\mathbf{r}, t) = sy\mathbf{e}_x$, where y and \mathbf{e}_x are the y -coordinate and unit vector along the x -axis, respectively. Here, the mean granular temperature is determined as

$$\theta_0 = \frac{a_\eta G(\phi) + b_\eta G(\phi)^{-1} + c_\eta}{16\pi^{-3/2}G(\phi)} \frac{s^2}{1 - e^2} \quad (31)$$

from Eq. (8). Then, we introduce small fluctuations around the homogeneous solution as

$$\phi(\mathbf{r}, t) = \phi_0 + \delta\phi(\mathbf{r}, t), \quad (32)$$

$$\theta(\mathbf{r}, t) = \theta_0 + \delta\theta(\mathbf{r}, t), \quad (33)$$

$$\mathbf{u}(\mathbf{r}, t) = sy\mathbf{e}_x + \delta\mathbf{u}(\mathbf{r}, t), \quad (34)$$

where $\delta\mathbf{u}(\mathbf{r}, t) = (\delta u_x, \delta u_y)$ is equivalent to the *non-affine velocity field*.

First, we expand the pressure, shear viscosity, and energy dissipation (which are the functions of ϕ and θ) into the series of small fluctuations as

$$p \approx p_0 + p_\phi \delta\phi + p_\theta \delta\theta + \dots, \quad (35)$$

$$\eta \approx \eta_0 + \eta_\phi \delta\phi + \eta_\theta \delta\theta + \dots, \quad (36)$$

$$\chi \approx \chi_0 + \chi_\phi \delta\phi + \chi_\theta \delta\theta + \dots, \quad (37)$$

respectively, where p_0 , η_0 , and χ_0 are the values for the homogeneous solution, i.e. $\phi = \phi_0$ and $\theta = \theta_0$, and explicit forms of the derivatives, p_α , η_α , and χ_α ($\alpha = \phi, \theta$) are listed in Table 3. Because we use the global fitting, Eq. (26), for the model of pair correlation function, its derivative in Table 3 is given by $dG(\phi)/d\phi = dG_{GF}(\phi)/d\phi$ with

$$\begin{aligned} \frac{dG_{GF}}{d\phi} &= \frac{dG_{CS}}{d\phi} + \\ &\frac{\left(\frac{dG_{FV}}{d\phi} - \frac{dG_{CS}}{d\phi}\right) + \left(\frac{dG_{FV}}{d\phi} - \frac{dG_{CS}}{d\phi} + \frac{G_{FV} - G_{CS}}{m_f}\right) \exp\left[-\frac{\phi - \phi_f}{m_f}\right]}{\left\{1 + \exp[-(\phi - \phi_f)/m_f]\right\}^2}, \end{aligned} \quad (38)$$

$$\frac{dG_{FV}}{d\phi} = \frac{\sqrt{\phi_\infty/\phi}}{2(1+e)\phi\left(\sqrt{\phi_\infty/\phi} - 1\right)^2}, \quad (39)$$

$$\frac{dG_{CS}}{d\phi} = \frac{1 + \frac{\phi}{8}}{(1 - \phi)^3}, \quad (40)$$

where we omit the arguments, “ (ϕ) ”, for the three different models, $G_{GF}(\phi)$, $G_{FV}(\phi)$, and $G_{CS}(\phi)$.

Second, we linearize the hydrodynamic equations (6)-(8) around the homogeneous solution. For example, each term on the right-hand-sides of Eqs. (7) and (8) is linearized as

p_ϕ	$= \frac{a_0}{\phi_\infty - \phi_0} + \left[1 + (1+e)(G_0 + \phi_0 G_\phi)\right] \theta_0$
p_θ	$= [1 + (1+e)G_0] \phi_0$
η_ϕ	$= \left[p_\phi f_{\eta 0} - p_0 \frac{df_\eta}{d\phi}\right] f_{\eta 0}^{-2} \theta_0^{-1/2}$
η_θ	$= \left[p_\theta \theta_0^{1/2} - \frac{p_0}{2\theta_0^{1/2}}\right] f_{\eta 0}^{-1} \theta_0^{-1}$
χ_ϕ	$= \left[p_\phi f_{\chi 0} - p_0 \frac{df_\chi}{d\phi}\right] f_{\chi 0}^{-2} \theta_0^{1/2}$
χ_θ	$= \left[p_\theta \theta_0^{1/2} + \frac{p_0}{2\theta_0^{1/2}}\right] f_{\chi 0}^{-1}$
$\frac{df_\eta}{d\phi}$	$= \frac{(1+e)(2b_\eta G_0^{-1} + c_\eta) - a_\eta + b_\eta G_0^{-2}}{(a_\eta G_0 + b_\eta G_0^{-1} + c_\eta)^2} G_\phi$
$\frac{df_\chi}{d\phi}$	$= -\frac{G_\phi}{a_\chi G_0^2}$

Table 3: Derivatives in the Taylor expansions, Eqs. (35)-(37), where $G_0 \equiv G(\phi_0)$, $f_{\eta 0} \equiv f_\eta(\phi_0)$, $f_{\chi 0} \equiv f_\chi(\phi_0)$, and $G_\phi \equiv dG(\phi)/d\phi|_{\phi=\phi_0}$.

follows:

$$\begin{aligned} \nabla_j \sigma_{xj} &\approx (s\eta_\phi \nabla_y - p_\phi \nabla_x) \delta\phi + (s\eta_\theta \nabla_y - p_\theta \nabla_x) \delta\theta \\ &+ (\eta_0 \nabla^2 + \xi_0 \nabla_x^2) \delta u_x + \xi_0 \nabla_x \nabla_y \delta u_y, \end{aligned}$$

$$\begin{aligned} \nabla_j \sigma_{yj} &\approx (s\eta_\phi \nabla_x - p_\phi \nabla_y) \delta\phi + (s\eta_\theta \nabla_x - p_\theta \nabla_y) \delta\theta \\ &+ (\eta_0 \nabla^2 + \xi_0 \nabla_y^2) \delta u_y + \xi_0 \nabla_x \nabla_y \delta u_x, \end{aligned}$$

$$\begin{aligned} \sigma_{ij} \nabla_i u_j &\approx \eta_0 s^2 + \eta_\phi s^2 \delta\phi + \eta_\theta s^2 \delta\theta \\ &+ (2s\eta_0 \nabla_y - p_0 \nabla_x) \delta u_x + (2s\eta_0 \nabla_x - p_0 \nabla_y) \delta u_y, \end{aligned}$$

$$\nabla_i q_i \approx -\kappa_0 \nabla^2 \delta\theta.$$

In the following, we introduce coefficients associated with the balance between external *supply of energy* by simple shear deformations and *energy dissipation* due to inelastic interactions as

$$\lambda_0 \equiv \eta_0 s^2 - \chi_0, \quad (41)$$

$$\lambda_\phi \equiv \eta_\phi s^2 - \chi_\phi, \quad (42)$$

$$\lambda_\theta \equiv \eta_\theta s^2 - \chi_\theta, \quad (43)$$

where all the second terms on the right-hand-sides are proportional to the inelasticity, $\chi_\alpha \propto 1 - e^2$ ($\alpha = 0, \phi, \theta$). Then, we find linearized hydrodynamic equations (or *linearized hydrodynamics*) as

$$\frac{\delta\delta\phi}{\delta t} + \epsilon y \nabla_x \delta\phi \approx -\phi_0 \nabla_i \delta u_i, \quad (44)$$

$$\begin{aligned} \frac{\delta\delta u_x}{\delta t} + \epsilon y \nabla_x \delta u_x &\approx (s\bar{\eta}_\phi \nabla_y - \bar{p}_\phi \nabla_x) \delta\phi + (s\bar{\eta}_\theta \nabla_y - \bar{p}_\theta \nabla_x) \delta\theta \\ &+ (\bar{\eta}_0 \nabla^2 + \bar{\xi}_0 \nabla_x^2) \delta u_x + (\bar{\xi}_0 \nabla_x \nabla_y - s) \delta u_y, \end{aligned} \quad (45)$$

$$\begin{aligned} \frac{\delta\delta u_y}{\delta t} + \epsilon y \nabla_x \delta u_y &\approx (s\bar{\eta}_\phi \nabla_x - \bar{p}_\phi \nabla_y) \delta\phi + (s\bar{\eta}_\theta \nabla_x - \bar{p}_\theta \nabla_y) \delta\theta \\ &+ (\bar{\eta}_0 \nabla^2 + \bar{\xi}_0 \nabla_y^2) \delta u_y + \bar{\xi}_0 \nabla_x \nabla_y \delta u_x, \end{aligned} \quad (46)$$

$$\begin{aligned} \frac{\delta\delta\theta}{\delta t} + \epsilon y \nabla_x \delta\theta &\approx \bar{\lambda}_\phi \delta\phi + (\bar{\lambda}_\theta + \bar{\kappa}_0 \nabla^2) \delta\theta \\ &+ (2s\bar{\eta}_0 \nabla_y - \bar{p}_0 \nabla_x) \delta u_x + (2s\bar{\eta}_0 \nabla_x - \bar{p}_0 \nabla_y) \delta u_y, \end{aligned} \quad (47)$$

where we introduced scaled quantities as $\bar{p}_\alpha \equiv p_\alpha/\phi_0$, $\bar{\xi}_0 \equiv \xi_0/\phi_0$, $\bar{\eta}_\alpha \equiv \eta_\alpha/\phi_0$, $\bar{\kappa}_0 \equiv \kappa_0/\phi_0$, and $\bar{\lambda}_\alpha \equiv \lambda_\alpha/\phi_0$ ($\alpha = 0, \phi, \theta$).

Assuming that non-affine velocities are isotropic in space, we seek normal mode solutions of the small fluctuations, i.e. $\delta\phi = \delta\hat{\phi}e^{i(ky-\omega t)}$, $\delta\theta = \delta\hat{\theta}e^{i(ky-\omega t)}$, $\delta u_x = i\delta\hat{u}_xe^{i(ky-\omega t)}$, and $\delta u_y = i\delta\hat{u}_ye^{i(ky-\omega t)}$, with the wave number, k , frequency, ω , and imaginary unit, i . Then, the linearized hydrodynamics, Eqs. (44)-(47), are reduced to an eigenvalue problem,

$$\mathcal{L}\hat{\phi} = -i\omega\hat{\phi}, \quad (48)$$

where the right-eigenvector is defined by the *hydrodynamic modes* as $\hat{\phi} = (\delta\hat{\phi}, \delta\hat{\theta}, \delta\hat{u}_x, \delta\hat{u}_y)^T$ and the 4×4 *hydrodynamic matrix* is given by

$$\mathcal{L} = \begin{pmatrix} 0 & 0 & 0 & \phi_0 k \\ \bar{\lambda}_\phi & \bar{\lambda}_\theta - \bar{\kappa}_0 k^2 & -2s\bar{\eta}_0 k & \bar{p}_0 k \\ s\bar{\eta}_\phi k & s\bar{\eta}_\theta k & -\bar{\eta}_0 k^2 & -s \\ -\bar{p}_\phi k & -\bar{p}_\theta k & 0 & -(\bar{\eta}_0 + \bar{\xi}_0)k^2 \end{pmatrix}. \quad (49)$$

For later use, we also define the left-eigenvector, $\hat{\psi}$, of the hydrodynamic matrix as

$$\hat{\psi}\mathcal{L} = -i\omega\hat{\psi}. \quad (50)$$

2.2 Perturbation theory

To determine the hydrodynamic modes, we perturbatively solve the eigenvalue problems, Eqs. (48) and (50). The perturbation theory which we adopt is well established for the linear stability analysis of granular gases under shear [53–55]. Because the power-law behavior of the spectrum, $E(k) \sim k^{-9/5}$, is observed in a *quasi-static regime*, $\dot{\gamma}t_m \ll 1$, we use the scaled shear rate, $s = \dot{\gamma}t_m$, as a small parameter for our perturbative calculations, i.e. $\epsilon \equiv s$. If the system is in a steady state, the external supply of energy by simple shear deformations must be canceled out by the energy dissipation in the bulk such that the mean granular temperature, θ_0 , stays constant (it should be compared with *thermostatted systems*, where the heat generated by the viscous heating is automatically removed from the system by the thermostats to keep the temperature constant). Therefore, from the equation of granular temperature, Eq. (8), we scale the energy dissipation as $\chi \sim \eta s^2 \sim \epsilon^2$. In addition, we scale the wave number as $k \sim \epsilon$ to understand the long wave-length behavior of the spectrum. Then, scaled forms of the wave number, k , and coefficients, $\lambda_\alpha = \eta_\alpha s^2 - \chi_\alpha$ (Eqs. (41)-(43)), are introduced as

$$k = \epsilon q, \quad \lambda_\alpha = \epsilon^2 \Lambda_\alpha, \quad (51)$$

($\alpha = 0, \phi, \theta$), respectively [53–55].

For the perturbative calculations of the eigenvalue problems, Eqs. (48) and (50), we expand the hydrodynamic matrix, eigenvalue, right- and left-eigenvectors into the power series of ϵ as

$$\mathcal{L} = \epsilon \mathcal{M}_1 + \epsilon^2 \mathcal{M}_2, \quad (52)$$

$$-i\omega = i\epsilon\omega_1 + \epsilon^2\omega_2 + \dots, \quad (53)$$

$$\hat{\phi} = \hat{\phi}_0 + \epsilon\hat{\phi}_1 + \epsilon^2\hat{\phi}_2 + \dots, \quad (54)$$

$$\hat{\psi} = \hat{\psi}_0 + \epsilon\hat{\psi}_1 + \epsilon^2\hat{\psi}_2 + \dots, \quad (55)$$

respectively, where the matrices in Eq. (52) are given by

$$\mathcal{M}_1 = \begin{pmatrix} 0 & 0 & 0 & \phi_0 q \\ 0 & 0 & 0 & \bar{p}_0 q \\ 0 & 0 & 0 & -1 \\ -\bar{p}_\phi q & -\bar{p}_\theta q & 0 & 0 \end{pmatrix}, \quad (56)$$

$$\mathcal{M}_2 = \begin{pmatrix} 0 & 0 & 0 & 0 \\ \bar{\Lambda}_\phi & \bar{\Lambda}_\theta - \bar{\kappa}_0 q^2 & -2\bar{\eta}_0 q & 0 \\ \bar{\eta}_\phi q & \bar{\eta}_\theta q & -\bar{\eta}_0 q^2 & 0 \\ 0 & 0 & 0 & -(\bar{\eta}_0 + \bar{\xi}_0)q^2 \end{pmatrix}, \quad (57)$$

with the scaled quantity, $\bar{\Lambda}_\alpha \equiv \Lambda_\alpha / \phi_0$ ($\alpha = \phi, \theta$).

2.2.1 The 1st order equation

Substituting the power series, Eqs. (52)-(55), into the eigenvalue problems, Eqs. (48) and (50), we find that the first order equations are given by

$$\mathcal{M}_1 \hat{\phi}_0^{(l)} = \omega_1^{(l)} \hat{\phi}_0^{(l)}, \quad (58)$$

$$\hat{\psi}_0^{(l)} \mathcal{M}_1 = \omega_1^{(l)} \hat{\psi}_0^{(l)}, \quad (59)$$

respectively ($l = 1, 2, 3, 4$). Then, the four eigenvalues are readily found to be

$$\omega_1^{(1)} = \omega_1^{(2)} = 0, \quad \omega_1^{(3)} = -\omega_1^{(4)} = Jq/\phi_0, \quad (60)$$

with a constant, $J \equiv \sqrt{\phi_0^2 p_\phi + p_0 p_\theta}$, where the corresponding right- and left-eigenvectors are given by

$$\hat{\phi}_0^{(1)} = (0, 0, 1, 0)^T, \quad (61)$$

$$\hat{\phi}_0^{(2)} = (-p_\theta/J, p_\phi/J, 0, 0)^T, \quad (62)$$

$$\hat{\phi}_0^{(3)} = (\phi_0^2/2J, p_0/2J, -\phi_0/2Jq, i/2)^T, \quad (63)$$

$$\hat{\phi}_0^{(4)} = (\phi_0^2/2J, p_0/2J, -\phi_0/2Jq, -i/2)^T, \quad (64)$$

and

$$\hat{\psi}_0^{(1)} = (\phi_0 p_\phi / J^2 q, \phi_0 p_\theta / J^2 q, 1, 0), \quad (65)$$

$$\hat{\psi}_0^{(2)} = (-p_0/J, \phi_0^2/J, 0, 0), \quad (66)$$

$$\hat{\psi}_0^{(3)} = (p_\phi/J, p_\theta/J, 0, -i), \quad (67)$$

$$\hat{\psi}_0^{(4)} = (p_\phi/J, p_\theta/J, 0, i), \quad (68)$$

respectively. Note that these eigenvectors satisfy the orthonormality, i.e. $\hat{\psi}_0^{(j)} \hat{\phi}_0^{(l)} = \delta_{jl}$ ($j = 1, 2, 3, 4$).

2.2.2 The 2nd order equation

Because the first and second eigenvalues are degenerated to zero, i.e. $\omega_1^{(1)} = \omega_1^{(2)} = 0$, we rewrite the right-eigenvectors, Eq. (54), for $l = 1, 2$ as

$$\hat{\phi}_0^{(l)} = a_j^{(l)} \hat{\phi}_0^{(j)} + \epsilon \hat{\phi}_1^{(l)} + \dots, \quad (69)$$

where $a_j^{(l)}$ is the coefficient for $\hat{\phi}_0^{(j)}$ and the Einstein convention is used for the index, $j = 1, 2$. Then, the second order equation is found to be

$$\mathcal{M}_1 \hat{\phi}_1^{(l)} + \mathcal{M}_2 a_j^{(l)} \hat{\phi}_0^{(j)} = \omega_2^{(l)} a_j^{(l)} \hat{\phi}_0^{(j)}. \quad (70)$$

If we multiply $\hat{\psi}_0^{(h)}$ ($h = 1, 2$) to the second order equation (70), the first term on the left-hand-side vanishes (since $\hat{\psi}_0^{(h)} \mathcal{M}_1 = 0$) and the equation is reduced to

$$\hat{\psi}_0^{(h)} \mathcal{M}_2 \hat{\varphi}_0^{(j)} a_j^{(l)} = \omega_2^{(l)} a_h^{(l)}, \quad (71)$$

where we used the orthonormality, $\hat{\psi}_0^{(h)} \hat{\varphi}_0^{(j)} = \delta_{hj}$. Note that if we rewrite the matrix elements on the left-hand-side of Eq. (71) as $m_{hj} \equiv \hat{\psi}_0^{(h)} \mathcal{M}_2 \hat{\varphi}_0^{(j)}$, Eq. (71) is explicitly written as

$$\begin{pmatrix} m_{11} & m_{12} \\ m_{21} & m_{22} \end{pmatrix} \begin{pmatrix} a_1^{(l)} \\ a_2^{(l)} \end{pmatrix} = \omega_2^{(l)} \begin{pmatrix} a_1^{(l)} \\ a_2^{(l)} \end{pmatrix}, \quad (72)$$

where each element is given by

$$m_{11} = -\frac{2\eta_0 p_\theta}{J^2} - \frac{\eta_0}{\phi_0} q^2, \quad (73)$$

$$m_{12} = \frac{p_\theta}{J^3} (p_\phi \Lambda_\theta - p_\theta \Lambda_\phi) q^{-1} + \left(\frac{p_\phi \eta_\theta - p_\theta \eta_\phi}{\phi_0 J} - \frac{\kappa_0 p_\phi p_\theta}{J^3} \right) q, \quad (74)$$

$$m_{21} = -\frac{2\phi_0 \eta_0}{J} q, \quad (75)$$

$$m_{22} = \frac{\phi_0}{J^2} (p_\phi \Lambda_\theta - p_\theta \Lambda_\phi) - \frac{\phi_0 \kappa_0 p_\phi}{J^2} q^2. \quad (76)$$

The two eigenvalues in Eq. (72) are readily found to be

$$\omega_2^{(1)} = \frac{1}{2} (m_{11} + m_{22} + F), \quad (77)$$

$$\omega_2^{(2)} = \frac{1}{2} (m_{11} + m_{22} - F), \quad (78)$$

with $F \equiv \sqrt{(m_{11} - m_{22})^2 + 4m_{12}m_{21}}$, where the normalized eigenvector for the first eigenvalue, $\hat{\varphi}_2^{(1)}$, is given by

$$\begin{pmatrix} a_1^{(1)} \\ a_2^{(1)} \end{pmatrix} = \begin{pmatrix} \frac{m_{22} - m_{11} - F}{\sqrt{(m_{22} - m_{11} - F)^2 + 4m_{21}^2}} \\ -\frac{2m_{21}}{\sqrt{(m_{22} - m_{11} - F)^2 + 4m_{21}^2}} \end{pmatrix}. \quad (79)$$

2.2.3 Hydrodynamic modes and the spectrum

To determine the first order right-eigenvector, $\hat{\varphi}_1^{(1)}$, we multiply $\hat{\varphi}_0^{(h)} \hat{\psi}_0^{(h)}$ ($h = 3, 4$) to the second order equation (70), where we find²

$$\omega_1^{(h)} \hat{\varphi}_1^{(1)} + \hat{\varphi}_0^{(h)} \hat{\psi}_0^{(h)} \mathcal{M}_2 \hat{\varphi}_0^{(j)} a_j^{(1)} = 0. \quad (80)$$

Therefore, the first order right-eigenvector is written as

$$\hat{\varphi}_1^{(1)} = - \sum_{h=3,4} \frac{1}{\omega_1^{(h)}} \hat{\varphi}_0^{(h)} \hat{\psi}_0^{(h)} \mathcal{M}_2 \hat{\varphi}_0^{(j)} a_j^{(1)}, \quad (81)$$

where the matrix elements, $m_{hj} \equiv \hat{\psi}_0^{(h)} \mathcal{M}_2 \hat{\varphi}_0^{(j)}$, are given by

$$m_{31} = m_{41} = \frac{p_\theta}{\phi_0^2} m_{21}, \quad (82)$$

$$m_{32} = m_{42} = \frac{p_\theta}{\phi_0^2} m_{22}, \quad (83)$$

²We used $\hat{\varphi}_0^{(h)} \hat{\psi}_0^{(h)} \mathcal{M}_1 \hat{\varphi}_1^{(1)} = \omega_1^{(h)} \hat{\varphi}_1^{(1)}$ and $\hat{\varphi}_0^{(h)} \hat{\psi}_0^{(h)} \omega_2^{(l)} a_j^{(l)} \hat{\varphi}_0^{(j)} = \hat{\varphi}_0^{(h)} \omega_2^{(l)} a_j^{(l)} \delta_{hj} = 0$ for $j = 1, 2$ and $h = 3, 4$.

respectively. Then, substituting m_{hj} , $a_j^{(1)}$, $\omega_1^{(h)}$, and $\hat{\varphi}_0^{(h)}$ to Eq. (81), we find the first order right-eigenvector as

$$\hat{\varphi}_1^{(1)} = (0, 0, 0, C)^T \quad (84)$$

with $C \equiv -(m_{21} a_1^{(1)} + m_{22} a_2^{(1)}) p_\theta / (\phi_0 J q)$. It is known that the other modes ($l = 2, 3, 4$) are immediately suppressed in granular flows under simple shear deformations [53–55].

In summary, the hydrodynamic modes truncated at the first order of ϵ is derived as

$$\begin{aligned} \hat{\varphi}^{(1)} &\simeq a_j^{(1)} \hat{\varphi}_0^{(j)} + \epsilon \hat{\varphi}_1^{(1)} \\ &= \left(-p_\theta a_2^{(1)} / J, p_\theta a_2^{(1)} / J, a_1^{(1)}, \epsilon C \right)^T, \end{aligned} \quad (85)$$

where the normalized energy spectrum, $E(k)/E(0) = \delta \hat{u}_x^2 + \delta \hat{u}_y^2$, is given by

$$\frac{E(k)}{E(0)} = a_1^{(1)2} + \epsilon^2 C^2. \quad (86)$$

In the manuscript, we denote $a_1^{(1)}$ and $a_2^{(1)}$ as $a_1(q)$ and $a_2(q)$, respectively.

2.3 Parameter dependence

We examine the sensitivity of our theoretical expression of the spectrum, Eq. (86), to the mean area fraction, ϕ_0 , the models of pair correlation functions, Eqs. (24)-(26), and the fitting parameter in Savage's theory, Eq. (30). We also discuss the dependence of our theoretical expression on the critical area fraction, ϕ_c , and maximum area fraction, ϕ_∞ , which we have already estimated from the numerical results of macroscopic flow properties of dense granular materials (Sec. 1.7).

Figure 5 shows the dependence of the theoretical expression, Eq. (86), on the mean area fraction in the range between $\phi_c < \phi_0 < \phi_\infty$, i.e. in a yielding state, where the global fitting, Eq. (26), is used for the model of pair correlation function, i.e. $G(\phi) = G_{GF}(\phi)$, and the parameters in Savage's continuum theory (a_0 , ϕ_c , and ϕ_∞) are determined by the numerical results of macroscopic flow properties as listed in Table 2. In this figure, there is no significant difference between the theoretical expressions with different values of the mean area fraction, as we have also confirmed in MD simulations that the spectrum is quite insensitive to the mean area fraction if the system is yielding, $\phi_0 > \phi_c$, in a quasi-static regime.

Figure 6 displays the theoretical expressions with the three different models of pair correlation functions, Eqs. (24)-(26), where the mean area fraction and scaled shear rate are fixed to $\phi_0 = 0.84$ and $\dot{\gamma} t_m = 2.5 \times 10^{-5}$, respectively, in both the MD simulations and theoretical expression, Eq. (86), such that the system is yielding in a quasi-static regime. In this figure, the theoretical expression is almost independent of the choice of pair correlation functions, except for the difference in high wave numbers, $kd_m \gtrsim 3$.

Figure 7 shows the dependence of the theoretical expression on the parameters introduced in Savage's continuum theory, i.e. (a) the reference value of contact pressure, a_0 , (b)

critical area fraction, ϕ_c , and (c) maximum area fraction, ϕ_∞ . As shown in Fig. 7(a), the theoretical expression is insensitive to the reference value (in the range between $0.025 \leq a_0/k_n \leq 0.125$). However, it increases with the increase of critical area fraction from $\phi_c = 0.70$ to 0.85 (Fig. 7(b)) and decreases with the increase of maximum area fraction from $\phi_\infty = 0.86$ to 0.92 (Fig. 7(c)). Note that the maximum area fraction, ϕ_∞ , are included not only in the constitutive model of pressure, p_{con} (Eq. (15)), but also in the model of pair correlation function at contact, $G_{\text{GF}}(\phi)$ (Eq. (26)). Therefore, the values of ϕ_c and ϕ_∞ are important in our theoretical expression of the spectrum, though these values can be determined from the numerical results of macroscopic flow properties of dense granular materials (Sec. 1.7).

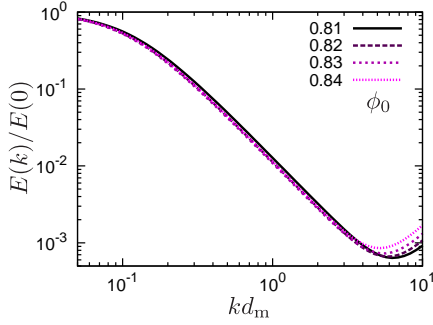


Figure 5: (Color online) The theoretical expression of the spectrum, Eq. (86), with different values of the mean area fraction, ϕ_0 , as listed in the legend, where the parameters in Savage's continuum theory (a_0 , ϕ_c , and ϕ_∞) are listed in Table 2. The global fitting model, Eq. (26), is used for the pair correlation function, i.e. $G(\phi) = G_{\text{GF}}(\phi)$.

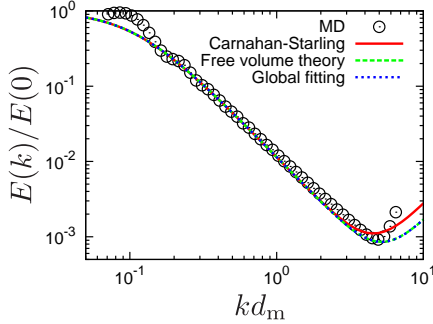


Figure 6: (Color online) The theoretical expression of the spectrum, Eq. (86), with three different models of pair correlation function at contact, $G(\phi)$, where the red solid, green broken, and blue dotted lines represent the Carnahan-Starling model, $G_{\text{CS}}(\phi)$, free volume theory, $G_{\text{FV}}(\phi)$, and global fitting, $G_{\text{GF}}(\phi)$, i.e. Eqs. (24)-(26), respectively (as listed in the legend). The parameters in Savage's continuum theory (a_0 , ϕ_c , and ϕ_∞) are listed in Table 2. The open circles are the result of MD simulations. In both the MD simulations and theoretical expression, Eq. (86), the mean area fraction and scaled shear rate are fixed to $\phi_0 = 0.84$ and $\dot{\gamma}t_m = 2.5 \times 10^{-5}$, respectively.

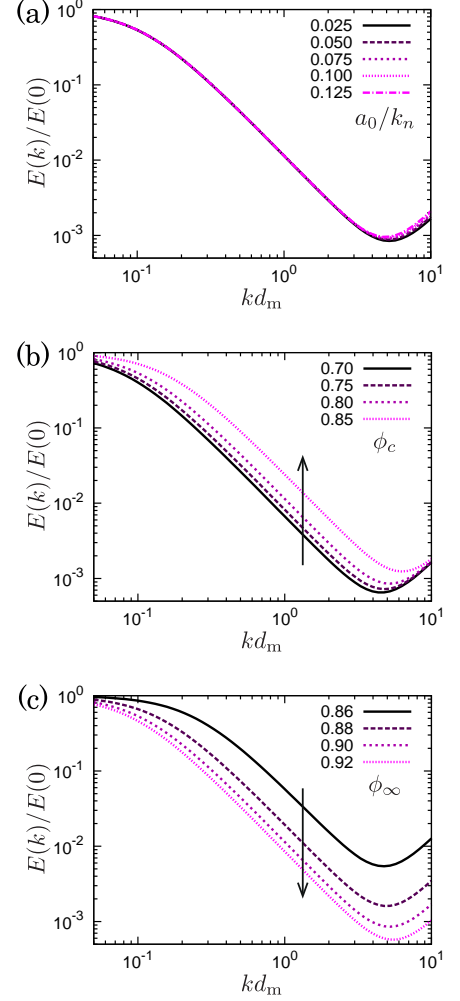


Figure 7: (Color online) The dependence of the theoretical expression, Eq. (86), on the parameters in Savage's continuum theory, i.e. a_0 , ϕ_c , and ϕ_∞ , where the mean area fraction and scaled shear rate are fixed to $\phi_0 = 0.84$ and $\dot{\gamma}t_m = 2.5 \times 10^{-5}$, respectively: (a) The reference value of contact pressure, a_0 , increases as listed in the legend (in the unit of spring constant, k_n), where $\phi_c = 0.80$ and $\phi_\infty = 0.90$ are used. (b) The critical area fraction, ϕ_c , increases as listed in the legend and indicated by the arrow, where $a_0 = 3.25 \times 10^{-2}k_n$ and $\phi_\infty = 0.90$ are used. (c) The maximum area fraction, ϕ_∞ , increases as listed in the legend and indicated by the arrow, where $a_0 = 3.25 \times 10^{-2}k_n$ and $\phi_c = 0.80$ are used.

3 The difference from turbulence

In this section, we describe the basic picture behind the anomalous cascade of kinetic energy which we observed in MD simulations. The decay of the spectrum is obviously different from the usual energy cascade in two-dimensional turbulence, i.e. $E(k) \sim k^{-3}$ [56]. To clarify such a difference, we first summarize the usual energy cascade (Sec. 3.1) and then explain a possible interpretation on the cascade of kinetic energy in dense granular materials based on Refs. [57, 58] (Sec. 3.2).

3.1 The usual energy cascade

To shortly explain the usual energy cascade, we first introduce the (incompressible) Navier-Stokes equation for the velocity field, $\mathbf{u}(\mathbf{r}, t)$, as [59]

$$\frac{D}{Dt} \mathbf{u} = -\rho_0^{-1} \nabla p + \nu \Delta \mathbf{u}, \quad (87)$$

where $D/Dt = \partial/\partial t + \mathbf{u} \cdot \nabla$, ρ_0 , p , and $\nu = \eta/\rho_0$ are the material derivative, mass density (constant), pressure, and kinematic viscosity, respectively. Because the Fourier component of pressure is given by $p_{\mathbf{k}} = -(\rho_0/k^2) \sum_{\mathbf{k}'} (\mathbf{k} \cdot \mathbf{u}_{\mathbf{k}'}) (\mathbf{k}' \cdot \mathbf{u}_{\mathbf{k}-\mathbf{k}'})$, the Fourier transform of the Navier-Stokes equation (87) is written as

$$\frac{\partial}{\partial t} \mathbf{u}_{\mathbf{k}} = -I \sum_{\mathbf{k}'} (\mathbf{k} \cdot \mathbf{u}_{\mathbf{k}-\mathbf{k}'}) \mathbf{u}_{\mathbf{k}'}^{\perp} - \nu k^2 \mathbf{u}_{\mathbf{k}}, \quad (88)$$

where I , \mathbf{k} (or \mathbf{k}'), $k \equiv |\mathbf{k}|$, and $\mathbf{u}_{\mathbf{k}}$ are the imaginary unit, wave number vector, wave number, and the Fourier component of the velocity field, respectively. On the right-hand-side of Eq. (88), the first term represents a *nonlinear coupling* of the velocity fields with different wave numbers, $\mathbf{u}_{\mathbf{k}-\mathbf{k}'}$ and $\mathbf{u}_{\mathbf{k}'}$, which induces the mesoscopic transport of kinetic energy, i.e. the *energy cascade*, where

$$\mathbf{u}_{\mathbf{k}'}^{\perp} \equiv \mathbf{u}_{\mathbf{k}'} - \hat{\mathbf{k}} (\hat{\mathbf{k}} \cdot \mathbf{u}_{\mathbf{k}'}) \quad (89)$$

with the unit vector, $\hat{\mathbf{k}} \equiv \mathbf{k}/k$, is perpendicular to the wave number vector, \mathbf{k} , i.e. $\mathbf{u}_{\mathbf{k}'}^{\perp}$ is the transverse component of $\mathbf{u}_{\mathbf{k}'}$. The first term on the right-hand-side of Eq. (88) indicates the *propagation* of $\mathbf{u}_{\mathbf{k}}$ (because of the imaginary unit, I) so that the nonlinear coupling does not dissipate the kinetic energy. In fact, the nonlinear coupling, $(\mathbf{k} \cdot \mathbf{u}_{\mathbf{k}-\mathbf{k}'}) \mathbf{u}_{\mathbf{k}'}^{\perp}$, results from the pressure gradient and convection term in *inertia*, $\rho_0 D\mathbf{u}/Dt$, where both conserve the energy. However, the second term, $-\nu k^2 \mathbf{u}_{\mathbf{k}}$, represents the *diffusion* of $\mathbf{u}_{\mathbf{k}}$ which causes the energy dissipation.

If the wave number is sufficiently high, $k \gg 1$, the second term on the right-hand-side of Eq. (88) is dominant. Then, the Navier-Stokes equation (88) is reduced to a diffusion-type,

$$\frac{\partial}{\partial t} \mathbf{u}_{\mathbf{k}} \simeq -\nu k^2 \mathbf{u}_{\mathbf{k}}, \quad (90)$$

where the velocity field decays exponentially as $\mathbf{u}_{\mathbf{k}} \propto e^{-\nu k^2 t}$. This is the energy dissipation (or *viscous heating*) in usual

fluids, where the rate of dissipation, νk^2 , increases with the increase of wave numbers, and vice versa.

Figure 8(a) shows a schematic picture of the usual energy cascade in turbulence, where the energy injection at macroscopic scale induces large-scale eddies which further generate smaller size eddies. The nonlinear coupling of different wave numbers transfers the external supply of energy to smaller scales without energy dissipation. At microscopic scale (the Kolmogorov length $\sim l_m$), the viscous heating is dominant and the transferred energy is finally dissipated into heat. In between the macro- and micro-scales, the power-law decay of energy spectrum can be observed, e.g. $E(k) \sim k^{-5/3}$ and k^{-3} in three and two dimensions, respectively [56, 59].

3.2 The cascade of kinetic energy in dense granular materials

In contrast to usual fluids, granular materials dissipate the kinetic energy by *inelastic interactions* between the particles in the contacts [57, 58]. Because the contact forces in the normal and tangential directions are modeled by the linear spring-dashpot, i.e.

$$f_n = k_n \xi_n - \eta_n \dot{\xi}_n, \quad (91)$$

$$f_t = k_t \xi_t - \eta_t \dot{\xi}_t, \quad (92)$$

respectively, the inelastic interactions are caused by the damping forces ($-\eta_n \dot{\xi}_n$ and $-\eta_t \dot{\xi}_t$) which are proportional to the *relative speeds* between the particles in contacts ($\dot{\xi}_n$ and $\dot{\xi}_t$).

Figure 8(b) displays a schematic picture of the cascade of kinetic energy in dense granular materials under simple shear deformations. At macroscopic scale, the external supply of energy by simple shear deformations generates large-scale *collective motions* (or vortex-like structures) of granular particles, e.g. as shown in Fig. 11(a), where relative speeds between the particles are quite small (because they move together) and thus the energy dissipation by inelastic interactions is negligible. The large-scale collective motions induce smaller size collective motions as the kinetic energy is transferred to smaller scales (from the blue to white regions in Fig. 8(b)). At microscopic scale (about particle diameter $\sim d_m$), however, granular particles cannot form vortex-like structures (due to the size of their own) and they move *randomly* rather than collectively (the red region in Fig. 8(b)), where relative speeds between them are considerably large so that the transferred kinetic energy is finally dissipated by inelastic interactions.

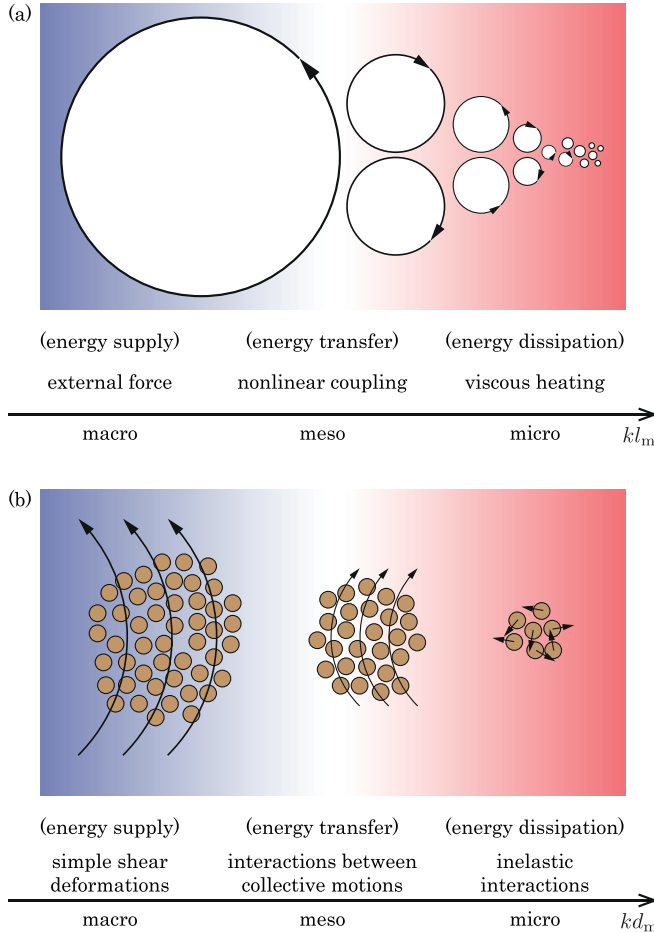


Figure 8: (Color online) (a) A sketch of the usual energy cascade, where the circles represent *eddies* rotating as indicated by the arrows and kl_m is the wave number scaled by the Kolmogorov length, l_m . External forces at macroscopic scale induce large-scale eddies (in the blue region) which further generate smaller size eddies (in the white and red regions). The nonlinear coupling of different wave numbers transfers the kinetic energy through the mesoscopic scales which is finally dissipated by the viscous heating at microscopic scale, $\sim l_m$. (b) A sketch of the “kinetic energy cascade” in dense granular materials, where the (filled) circles represent granular particles moving as indicated by the arrows and kd_m is the wave number scaled by the mean particle diameter, d_m . Simple shear deformations at macroscopic scale induce large-scale *collective motions* (in the blue region) which further generate smaller size collective motions (in the white region), while the particle motions are random at microscopic scale (in the red region). The interaction between different size of collective motions transfers the kinetic energy through the mesoscopic scales which is finally dissipated by the inelastic interactions at microscopic scale, $\sim d_m$.

4 Supplementary data

In this section, we provide some supplementary data of MD simulations for the manuscript. In Sec. 4.1, we show our

numerical results of the PDFs of non-affine velocities with different values of the control parameters, i.e. the mean area fraction, ϕ_0 , and scaled shear rate, $\dot{\gamma}t_m$. In Sec. 4.2, we confirm that the statistics of non-affine velocities, i.e. the PDFs, correlation functions, and spectra, are quite insensitive to the *microscopic friction coefficient*, μ_m , if the system is yielding ($\phi_0 > \phi_c$) in a quasi-static regime ($\dot{\gamma}t_m \ll 1$). In Sec. 4.3, we examine the effect of *particle inertia* on the power-law decay of the spectrum.

4.1 The dependence of the PDFs on the control parameters

Figure 9(a) displays the dependence of the PDFs on the mean area fraction, ϕ_0 , where the PDFs of each component, $P(\delta u_\alpha)$ with $\alpha = x, y$, are symmetric around zero ($\delta u_\alpha = 0$) and well correspond with each other (if ϕ_0 is the same) such that the distribution of non-affine velocities is *isotropic* in space. In this figure, the widths of the PDFs increase with ϕ_0 , while the difference between them becomes quite small once the mean area fraction exceeds the critical value, $\phi_0 > \phi_c$, i.e. if the system is yielding (or jammed).

Figure 9(b) shows the dependence of the PDFs on the scaled shear rate, $\dot{\gamma}t_m$, where the widths of the PDFs monotonously increase with the decrease of scaled shear rate, implying the growth of spatial correlations of non-affine velocities in a quasi-static regime, $\dot{\gamma}t_m \ll 1$.

The dependence of the widths of the PDFs on the control parameters should be compared with the results of spatial correlation functions of non-affine velocities in the manuscript, where the correlation length suddenly increases around the critical area fraction, $\phi_c \simeq 0.8$, and it monotonously increases with the decrease of scaled shear rate. Therefore, the increase of the width is closely related to the growth of spatial correlations of non-affine velocities.

4.2 The effect of microscopic friction on statistics of non-affine velocities

Figure 10 shows the dependence of the PDFs, $P(\delta u_y)$, correlation functions, $C(r)$, and spectra, $E(k)$, on the threshold for the Coulomb friction, where the microscopic friction coefficient varies from $\mu_m = 0.1$ to 0.5. In Figs. 10(a) and (b), we confirm that the PDFs and correlation functions are quite insensitive to the microscopic friction if the system is yielding in a quasi-static regime ($\phi_0 = 0.84$ and $\dot{\gamma}t_m = 2.5 \times 10^{-5}$). In addition, there is no significant difference between the spectra such that the power-law behavior, $E(k) \sim k^{-9/5}$, is well retained in the range between $0.1 \leq \mu_m \leq 0.5$ (Fig. 10(c)).

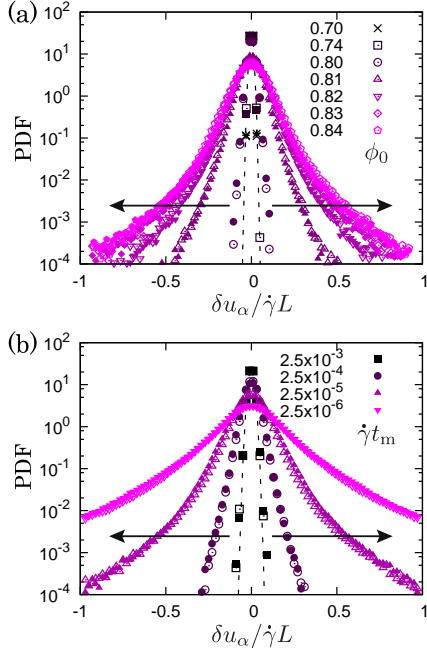


Figure 9: (Color online) (a) The dependence of the PDFs on the mean area fraction, ϕ_0 , where ϕ_0 increases as listed in the legend and indicated by the arrows. The scaled shear rate is fixed to $\dot{\gamma} t_m = 2.5 \times 10^{-5}$ and the dotted line represents a Gaussian fit for $P(\delta u_x)$ with the smallest mean area fraction, $\phi_0 = 0.70$. (b) The dependence of the PDFs on the scaled shear rate, $\dot{\gamma} t_m$, where $\dot{\gamma} t_m$ decreases as listed in the legend and indicated by the arrows. The mean area fraction is fixed to $\phi_0 = 0.84$ and the dotted line represents a Gaussian fit for $P(\delta u_x)$ with the largest shear rate, $\dot{\gamma} t_m = 2.5 \times 10^{-3}$. In both (a) and (b), the closed and open symbols represent $P(\delta u_x)$ and $P(\delta u_y)$, respectively, and the microscopic friction coefficient is given by $\mu_m = 0.5$.

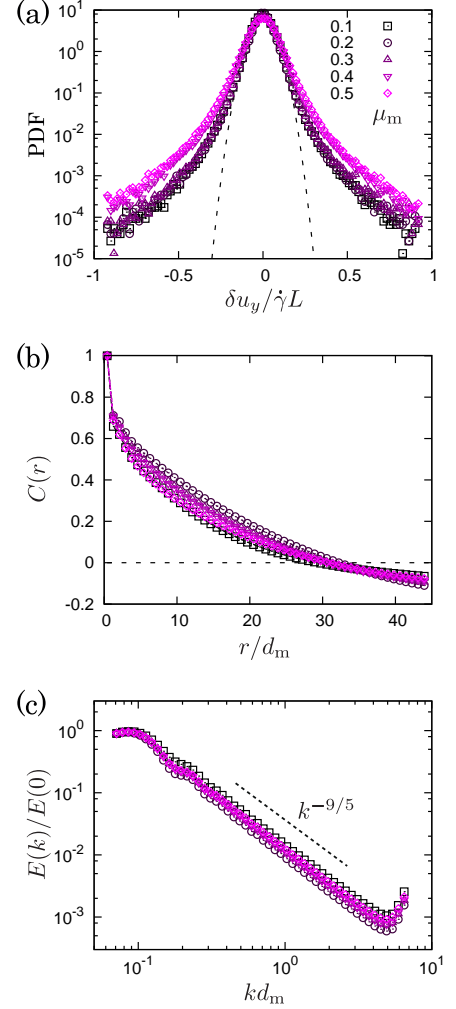


Figure 10: (Color online) Effects of microscopic friction on the (a) PDFs, (b) correlation functions, and (c) spectra of non-affine velocities, where the microscopic friction coefficient, μ_m , increases as listed in the legend of (a). The dotted line in (a) represents a Gaussian fit for the result of the smallest microscopic friction coefficient, $\mu_m = 0.1$. Here, the mean area fraction and scaled shear rate are fixed to $\phi_0 = 0.84$ and $\dot{\gamma} t_m = 2.5 \times 10^{-5}$, respectively.

4.3 The effect of particle inertia

As shown in Sec. 3.1, the *inertia* plays a key role in the mesoscopic transport of kinetic energy in usual turbulent flows. However, the effect of *particle inertia* on the power-law decay of the spectrum in dense granular materials is still unknown.

To clarify the role of particle inertia, we carry out MD simulations with *overdamped dynamics*. In the manuscript, we numerically solved rigid body dynamics of each particle, i.e. numerically integrated the equations of translational and rotational motions. Now, we add *viscous forces* to the equations of motions as

$$m\dot{\mathbf{r}}_i = \sum_{j \neq i} \mathbf{f}_{ij} - \zeta_{\text{tra}} \dot{\mathbf{r}}_i, \quad (93)$$

$$I_i \dot{\omega}_i = \sum_{j \neq i} \mathbf{f}_{ij} \times \mathbf{n}_{ij} - \zeta_{\text{rot}} \omega_i, \quad (94)$$

($i, j = 1, \dots, N$), where we have introduced viscosity coefficients to the translational and rotational motions as ζ_{tra} and ζ_{rot} , respectively. In these equations, the contact force, \mathbf{f}_{ij} , is modeled by the linear spring-dashpot model (as described in the manuscript) and the particle angular velocity, ω_i , is driven by the torque between the particles in contacts, $\mathbf{f}_{ij} \times \mathbf{n}_{ij}$, where $\mathbf{n}_{ij} \equiv (\mathbf{r}_i - \mathbf{r}_j)/|\mathbf{r}_i - \mathbf{r}_j|$ is a unit vector parallel to the relative position. We set the particle mass, m , and the particle moment of inertia, $I_i \propto m$, to be zero and then numerically integrate overdamped dynamics,

$$\dot{\mathbf{r}}_i = \zeta_{\text{tra}}^{-1} \sum_{j \neq i} \mathbf{f}_{ij}, \quad (95)$$

$$\omega_i = \zeta_{\text{rot}}^{-1} \sum_{j \neq i} \mathbf{f}_{ij} \times \mathbf{n}_{ij}, \quad (96)$$

where we simply assume that the viscosity coefficients are the same, $\zeta_{\text{tra}} = \zeta_{\text{rot}} = 10mt_m^{-1}$.

We compare the overdamped dynamics ($m = I_i = 0$) with the underdamped dynamics ($\zeta_{\text{tra}} = \zeta_{\text{rot}} = 0$) which we originally used in the manuscript. Figure 11 shows spatial distributions of non-affine velocities obtained by the (a) underdamped dynamics and (b) overdamped dynamics, where the color coordinates are the same with that used in Fig. 1(b) of the manuscript. In this figure, we can see that the collective behavior of non-affine velocities is *extremely suppressed by the overdamped dynamics* and thus turbulent-like structures (e.g. large scale and small scale eddies) of non-affine velocities can be hardly observed. As a result, the spatial correlation function, $C(r)$, quickly decay (Fig. 12(a)) and the spectrum, $E(k)$, does not show a clear power-law decay (Fig. 12(b)) if we use the overdamped dynamics in MD simulations. Therefore, the particle inertia is crucial for the mesoscopic transport of kinetic energy in dense granular materials.

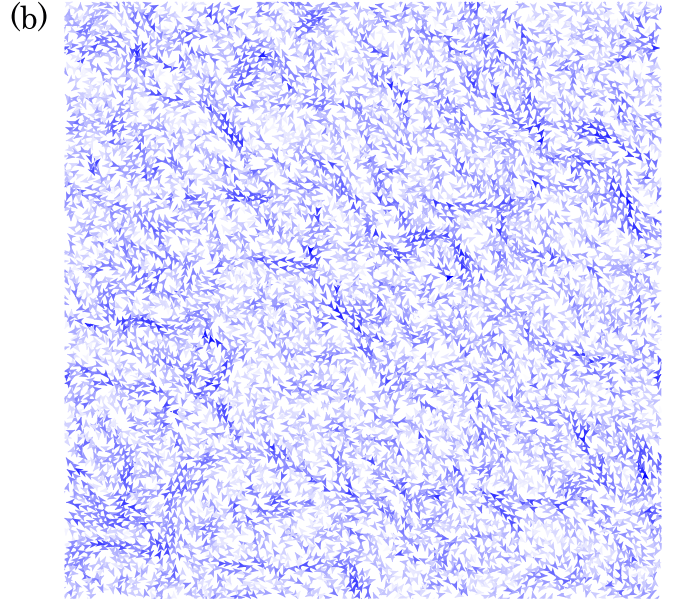
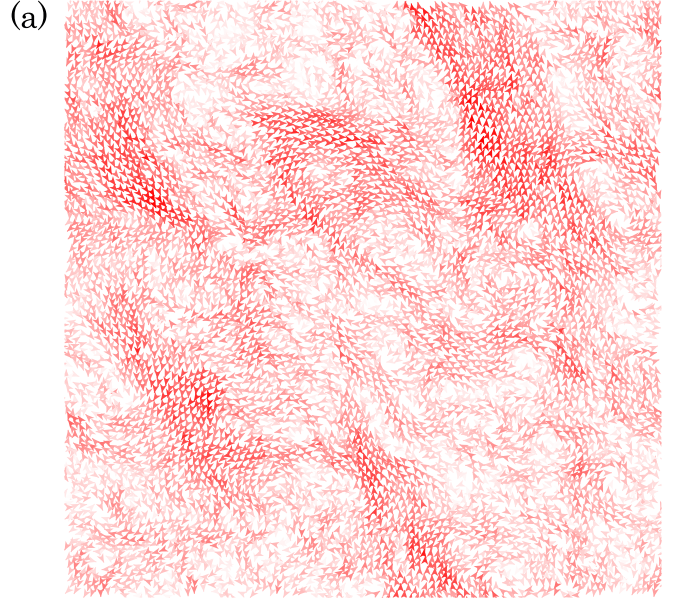


Figure 11: (Color online) Spatial distributions of non-affine velocities in steady states, where the color coordinates represent their magnitudes scaled by the maximum. The (a) underdamped dynamics and (b) overdamped dynamics are used in MD simulations, where the mean area fraction, scaled shear rate, and microscopic friction coefficient are fixed to $\phi_0 = 0.82$, $\dot{\gamma}t_m = 2.5 \times 10^{-5}$, and $\mu_m = 0.5$, respectively.

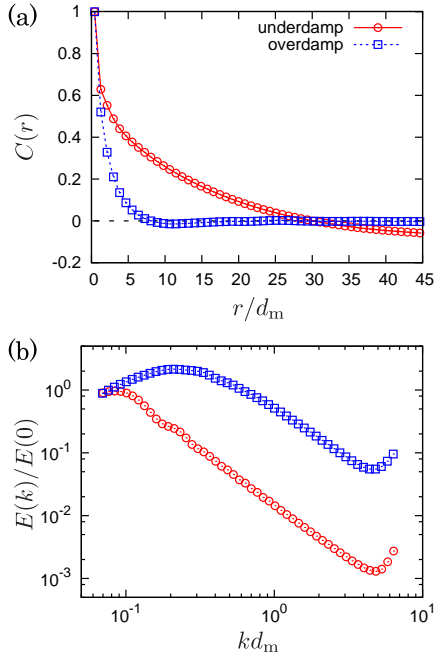


Figure 12: (Color online) (a) Spatial distribution functions and (b) spectra of non-affine velocities, where the underdamped dynamics (circles) and overdamped dynamics (squares) are used in MD simulations. The control parameters, i.e. ϕ_0 , $\dot{\gamma}t_m$, and μ_m , are as in Fig. 11.

References

- [1] S. B. Savage. *J. Fluid Mech.*, 377:1, 1998.
- [2] P. Olsson and S. Teitel. *Phys. Rev. Lett.*, 99:178001, 2007.
- [3] T. Hatano, M. Otsuki, and S. Sasa. *J. Phys. Soc. Japan*, 76:023001, 2007.
- [4] T. Hatano. *J. Phys. Soc. Japan*, 77:123002, 2008.
- [5] M. Otsuki and H. Hayakawa. *Phys. Rev. E*, 80:011308, 2009.
- [6] M. Otsuki and H. Hayakawa. *Prog. Theor. Phys.*, 121:647, 2009.
- [7] T. Hatano. *Prog. Theor. Phys. Suppl.*, 184:143, 2010.
- [8] K. N. Nordstrom, E. Verneuil, P. E. Arratia, A. Basu, Z. Zhang, A. G. Yodh, J. P. Gollub, and D. J. Durian. *Phys. Rev. Lett.*, 105:175701, 2010.
- [9] N. V. Brilliantov and T. Pöschel. *Kinetic Theory of Granular Gases*. Oxford University Press, Oxford, 2004.
- [10] C. K. W. Lun, S. B. Savage, D. J. Jeffrey, and N. Chepur-niy. *J. Fluid Mech.*, 140:223, 1984.
- [11] J. T. Jenkins and M. W. Richman. *Phys. Fluids*, 28:3485, 1985.
- [12] J. T. Jenkins and M. W. Richman. *Arch. Ration. Mech. Anal.*, 87:355, 1985.
- [13] C. K. K. Lun. *J. Fluid Mech.*, 233:539, 1991.
- [14] J. J. Brey, J. W. Dufty, and A. Santos. *J. Stat. Phys.*, 87:1051, 1997.
- [15] J. J. Brey, J. W. Dufty, C. S. Kim, and A. Santos. *Phys. Rev. E*, 58:4638, 1998.
- [16] V. Garzó and J. W. Dufty. *Phys. Rev. E*, 59:5895, 1999.
- [17] J. F. Lutsko. *Phys. Rev. E*, 72:021306, 2005.
- [18] D. Berzi and J. T. Jenkins. *Soft Matter*, 11:4799, 2015.
- [19] R. Yamamoto and A. Onuki. *Phys. Rev. E*, 58:3515, 1998.
- [20] O. Dauchot, G. Marty, and G. Biroli. *Phys. Rev. Lett.*, 95:265701, 2005.
- [21] G. Marty and O. Dauchot. *Phys. Rev. Lett.*, 94:015701, 2005.
- [22] M. Tsamados. *Eur. Phys. J. E*, 32:165, 2010.
- [23] K. N. Nordstrom, J. P. Gollub, and D. J. Durian. *Phys. Rev. E*, 84:021403, 2011.
- [24] T. Hatano. *J. Phys. Conf. Ser.*, 319:012011, 2011.
- [25] A. Furukawa and H. Tanaka. *Phys. Rev. E*, 84:061503, 2011.
- [26] A. Furukawa and H. Tanaka. *Phys. Rev. E*, 86:030501(R), 2012.
- [27] G. D. R. MiDi. *Eur. Phys. J. E*, 14:341, 2004.
- [28] F. da Cruz, S. Emam, M. Prochnow, J.-N. Roux, and F. Chevoir. *Phys. Rev. E*, 72:021309, 2005.
- [29] P. Jop, Y. Forterre, and O. Pouliquen. *Nature*, 441:727, 2006.
- [30] T. Hatano. *Phys. Rev. E*, 75:060301(R), 2007.
- [31] D. Berzi, C. G. di Prisco, and D. Vescovi. *Phys. Rev. E*, 84:031301, 2011.
- [32] F. Boyer, É. Guazzelli, and O. Pouliquen. *Phys. Rev. Lett.*, 107:188301, 2011.
- [33] E. Azéma and F. Radjaï. *Phys. Rev. Lett.*, 107:188301, 2011.
- [34] K. Kamrin and G. Koval. *Phys. Rev. Lett.*, 108:178301, 2012.
- [35] M. Bouzid, M. Trulsson, P. Claudin, E. Clément, and B. Andreotti. *Phys. Rev. Lett.*, 111:238301, 2013.

- [36] D. L. Henann and K. Kamrin. *PNAS*, 110:6730, 2013.
- [37] S. A. Hill and G. F. Mazenko. *Phys. Rev. E*, 63:031303, 2001.
- [38] I. S. Aranson and L. S. Tsimring. *Phys. Rev. E*, 64:020301(R), 2001.
- [39] J. Wakou, R. Brito, and M. H. Ernst. *J. Stat. Phys.*, 107:3, 2002.
- [40] I. S. Aranson and L. S. Tsimring. *Phys. Rev. E*, 65:061303, 2002.
- [41] D. Volfson, L. S. Tsimring, and I. S. Aranson. *Phys. Rev. Lett.*, 90:254301, 2003.
- [42] D. Volfson, L. S. Tsimring, and I. S. Aranson. *Phys. Rev. E*, 68:021301, 2003.
- [43] D. Volfson, L. S. Tsimring, and I. S. Aranson. *Phys. Rev. E*, 69:031302, 2004.
- [44] I. S. Aranson, F. Malloggi, and E. Clément. *Phys. Rev. E*, 73:050302(R), 2006.
- [45] I. S. Aranson, L. S. Tsimring, F. Malloggi, and E. Clément. *Phys. Rev. E*, 78:031303, 2008.
- [46] J. Lemaitre and J.-L. Chaboche. *Mechanics of Solid Materials*. Cambridge University Press, Cambridge, UK, 1990.
- [47] M. Otsuki and H. Hayakawa. *Phys. Rev. E*, 83:051301, 2011.
- [48] R. Seto, R. Mari, J. F. Morris, and M. M. Denn. *Phys. Rev. Lett.*, 111:218301, 2013.
- [49] M. Grob, C. Heussinger, and A. Zippelius. *Phys. Rev. E*, 89:050201(R), 2014.
- [50] M. Wyart and M. E. Cates. *Phys. Rev. Lett.*, 112:098302, 2014.
- [51] R. Mari, R. Seto, J. F. Morris, and M. M. Denn. *Phys. Rev. E*, 91:052302, 2013.
- [52] S. Luding. *Phys. Rev. E*, 63:042201, 2001.
- [53] K. Saitoh and H. Hayakawa. *Granular Matter*, 13:697, 2011.
- [54] K. Saitoh and H. Hayakawa. *Phys. Fluids*, 25:070606, 2013.
- [55] K. Saitoh, S. Takada, and H. Hayakawa. *Soft Matter*, 11:6371, 2015.
- [56] G. Boffetta and R. E. Ecke. *Annu. Rev. Fluid Mech.*, 44:427, 2012.
- [57] F. Radjai and S. Roux. *Phys. Rev. Lett.*, 89:064302, 2002.
- [58] E. Woldhuis, V. Chikkadi, M. S. van Deen, P. Schall, and M. van Hecke. *Soft Matter*, 11:7024, 2015.
- [59] U. Frisch. *Turbulence, the Legacy of A. N. Kolmogorov*. Cambridge University Press, Cambridge, UK, 1995.